

High-order harmonic generation of ZnO crystals in chirped and static electric fields

Ling-Yu Zhang(张玲玉), Yong-Lin He(何永林), Zhuo-Xuan Xie(谢卓璇), Fang-Yan Gao(高芳艳), Qing-Yun Xu(徐清芸), Xin-Lei Ge(葛鑫磊), Xiang-Yi Luo(罗香怡), and Jing Guo(郭静)
Citation: Chin. Phys. B, 2024, 33 (**1**): 013102. DOI: 10.1088/1674-1056/acfa89
Journal homepage: http://cpb.iphy.ac.cn; http://iopscience.iop.org/cpb

What follows is a list of articles you may be interested in

Review on typical applications and computational optimizations based on semiclassical methods in strong-field physics

Xun-Qin Huo(火勋琴), Wei-Feng Yang(杨玮枫), Wen-Hui Dong(董文卉), Fa-Cheng Jin(金发成), Xi-Wang Liu(刘希望), Hong-Dan Zhang(张宏丹), and Xiao-Hong Song(宋晓红)
Chin. Phys. B, 2022, 31 (**3**): 033101. DOI: 10.1088/1674-1056/ac306b

Complex coordinate rotation method based on gradient optimization

Zhi-Da Bai(白志达), Zhen-Xiang Zhong(钟振祥), Zong-Chao Yan(严宗朝), and Ting-Yun Shi(史庭云)
Chin. Phys. B, 2021, 30 (**2**): 023101. DOI: 10.1088/1674-1056/abc156

Theoretical analysis of the coupling between Feshbach states and hyperfine excited states in the creation of $^{23}Na^{40}K$ molecule

Ya-Xiong Liu(刘亚雄), Bo Zhao(赵博)
Chin. Phys. B, 2020, 29 (**2**): 023103. DOI: 10.1088/1674-1056/ab6314

Effect of electron correlation on high-order harmonic generation in helium model atom

Hu Shi-Lin (胡师林), Shi Ting-Yun (史庭云)
Chin. Phys. B, 2013, 22 (**1**): 013101. DOI: 10.1088/1674-1056/22/1/013101

Investigation of multiphoton and tunneling ionization of atoms in intense laser field

Fu Yan-Zhuo (付妍卓), Zhao Song-Feng (赵松峰), Zhou Xiao-Xin (周效信)
Chin. Phys. B, 2012, 21 (**11**): 113101. DOI: 10.1088/1674-1056/21/11/113101

High-order harmonic generation of ZnO crystals in chirped and static electric fields

Ling-Yu Zhang(张玲玉)[1], Yong-Lin He(何永林)[2,3], Zhuo-Xuan Xie(谢卓璇)[1], Fang-Yan Gao(高芳艳)[1], Qing-Yun Xu(徐清芸)[1], Xin-Lei Ge(葛鑫磊)[4], Xiang-Yi Luo(罗香怡)[5,†], and Jing Guo(郭静)[1,‡]

[1] *Institute of Atomic and Molecular Physics, Jilin University, Changchun* 130012, *China*
[2] *School of Physics and Electromechanical Engineering, Hexi University, Zhangye* 734000, *China*
[3] *Institute of Theoretical Physics, Hexi University, Zhangye* 734000, *China*
[4] *College of Physical Science and Technology, Bohai University, Jinzhou* 121013, *China*
[5] *College of Physics and Electronic Information, Baicheng Normal University, Baicheng* 137000, *China*

(Received 23 July 2023; revised manuscript received 7 September 2023; accepted manuscript online 18 September 2023)

High harmonic generation in ZnO crystals under chirped single-color field and static electric field are investigated by solving the semiconductor Bloch equation (SBE). It is found that when the chirp pulse is introduced, the interference structure becomes obvious while the harmonic cutoff is not extended. Furthermore, the harmonic efficiency is improved when the static electric field is included. These phenomena are demonstrated by the classical recollision model in real space affected by the waveform of laser field and inversion symmetry. Specifically, the electron motion in k-space shows that the change of waveform and the destruction of the symmetry of the laser field lead to the incomplete X-structure of the crystal-momentum-resolved (k-resolved) inter-band harmonic spectrum. Furthermore, a pre-acceleration process in the solid four-step model is confirmed.

Keywords: high-order harmonic generation, the semiconductor Bloch equation, k-resolved inter-band harmonic spectrum, four-step semiclassical model

PACS: 42.50.Ct,31.15.–p,31.15.xg **DOI:** 10.1088/1674-1056/acfa89

1. Introduction

High-order harmonics generation (HHG) driven by laser not only is a special nonlinear optical phenomenon, but also has become an important way to make extreme UV or soft x-ray band light source and desktop attosecond light source in the laboratory,[1,2] which provides a feasible scheme for synthesizing attosecond pulses to observe the internal electron dynamics of atoms and molecules, and also makes it possible to further explore and control microscopic particles. The physical mechanism of HHG is mainly given by the semi-classical three-step model proposed by Corkum in 1993.[3] In 2019, Lu *et al.*[4] proposed a four-step model to study HHG in solids, which can be explained as follows: (i) Electrons in the valence band are accelerated by a laser field. (ii) Tunneling excitation occurs at the minimum band gap. (iii) Subsequently, electron and hole pairs accelerate within the band. (iv) Finally, electron and hole recombine and emit harmonic photons with band-gap energy. Compared with the three-step model, the four-step model mainly has a pre-acceleration process. In 2020, Song *et al.*[5] studied ZnO driven by multi-color pulses to enhance HHG, and proved the occurrence of intra-band pre-acceleration, which confirmed the proposed four-step model of HHG from semiconductor.

Based on the research of high harmonics in gas, the description of the harmonic radiation process in solids is gradually perfected, and compared with the electron dynamics process in gas, there is a bit of differences for ultrafast electron dynamics in solids. In order to improve the harmonic efficiency and to extend the high-order harmonic spectrum, researchers have taken many methods in research of high-order harmonic generation from gas, such as using the chirp to control the laser waveform and controlling the dynamics of HHG. Spatially inhomogeneous fields,[6] two-color field,[7] and its combination with chirped pulse,[8,9] as well as the combination of static electric field and chirp[9,10] are used to extend the cutoff energy. For example, Mohebbi[11] used the combination of chirped laser pulse, non-chirped laser pulse and static electric field to drive helium atoms to enhance HHG, and then synthesized a clean 38 as isolated attosecond pulse. Liu *et al.*[12] introduced a two-color chirped pulse to extend the platform of HHG, and also added a controlled IR or UV pulse to improve the harmonic efficiency. Koushki *et al.*[9] showed that adding a static electric field to a two-color chirped laser field can significantly increase the harmonic cutoff and obtain pulses with a minimum duration of 21 as.

However, the emission of high harmonics driven by combined fields in solids needs to be further studied. Since the HHG process in solids is more complicated than that in atoms, which is due to the coincident movement of electrons and holes in the conduction band and valence band in

†Corresponding author. E-mail: luoxylgq@163.com
‡Corresponding author. E-mail: gjing@jlu.edu.cn

© 2024 Chinese Physical Society and IOP Publishing Ltd

solids,[13–17] the interference between high harmonics emitted by different channels,[18] or between inter-band and intra-band currents.[19] Based on this, we study the HHG of the combined field along the Γ–M direction of the ZnO crystal by solving the SBEs. The characteristics of harmonic spectra are analyzed based on the recollision model. Moreover, k-resolved inter-band harmonic spectra are also given. The incomplete X-structure of the inter-band harmonic spectrum can be analyzed by the four-step model.

In the rest of this paper, we present the theoretical method used here in Section 2. The calculation results and discussion are given in Section 3. Finally, the conclusions are given in Section 4. Atomic units are used throughout the text unless stated otherwise.

2. Theoretical method

HHG in solids can be investigated by many theoretical methods, such as the time-dependent Schrödinger equation (TDSE),[20–25] the time-dependent density functional theory (TDDFT),[26–31] and the semiconductor Bloch equation (SBE).[32–38] In this paper, we use SBEs to simulate HHG in solids:[14,15,39,40]

$$\dot{n}_m = \mathrm{i}\sum_{m'\neq m}\Omega_{mm'}\pi_{mm'}\,\mathrm{e}^{\mathrm{i}S_{mm'}} + \mathrm{c.c.}, \tag{1}$$

$$\begin{aligned}\dot{\pi}_{mm'} =& -\frac{\pi_{mm'}}{T_2} + \mathrm{i}\Omega^*_{mm'}(n_m - n_{m'})\,\mathrm{e}^{-\mathrm{i}S_{mm'}} \\ &+ \mathrm{i}\sum_{m''\notin\{m,m'\}}\Big(\Omega_{m'm''}\pi_{mm''}\,\mathrm{e}^{\mathrm{i}S_{m'm''}} \\ &- \Omega^*_{mm''}\pi^*_{m'm''}\,\mathrm{e}^{-\mathrm{i}S_{mm''}}\Big).\end{aligned} \tag{2}$$

Our simulation is based on a two-band model, including a valence band and a conduction band. Therefore in Eq. (1) $n_{m=\mathrm{v,c}}$ represents band population, v and c refer to valence band and conduction band, respectively, and $\pi_{mm'}(\boldsymbol{K},t)$ represents the quantum coherence between valence band and conduction band. $\Omega_{mm'}(\boldsymbol{K},t) = \boldsymbol{E}(t)\cdot d_{mm'}[\boldsymbol{K}+\boldsymbol{A}(t)]$ is the Rabi frequency, where $\boldsymbol{E}(t)$ is the electric field and $d_{mm'}[\boldsymbol{K}+\boldsymbol{A}(t)]$ is the momentum-dependent transition dipole moment of the crystal between the two bands. Here, $\mathrm{e}^{\mathrm{i}S_{mm'}}$ is the phase term, and $S_{mm'}(\boldsymbol{K},t) = \int_{-\infty}^{t}\{\varepsilon_m[\boldsymbol{K}+\boldsymbol{A}(t')] - \varepsilon_{m'}[\boldsymbol{K}+\boldsymbol{A}(t')]\}\,\mathrm{d}t'$ is the classical action, ε_m and $\varepsilon_{m'}$ refer to band energy, and T_2 is the dephasing time. According to Bloch's acceleration theorem, crystal momentum $\boldsymbol{K}(t) = \boldsymbol{k} - \boldsymbol{A}(t)$ is in a moving coordinate system, $\boldsymbol{K}(t)$ is the time-dependent momentum under the laser field, $\boldsymbol{k}$ is the initial momentum, $\boldsymbol{A}(t) = -\int_{-\infty}^{t}\boldsymbol{E}(t')\,\mathrm{d}t'$ is the vector potential of the laser field. In the semiconductor Bloch equations, we are using $\boldsymbol{K}+\boldsymbol{A}(t)$ to denote $\boldsymbol{k}$, and $\boldsymbol{A}(t)$ depends on t, so the variables are represented only by $\boldsymbol{K}$ and t. The polarization, which represents the polarizability between two energy bands, is defined as[14]

$$\boldsymbol{p}_{mm'}(\boldsymbol{K},t) = d_{mm'}(\boldsymbol{K},t)\pi_{mm'}(\boldsymbol{K},t)\,\mathrm{e}^{\mathrm{i}S_{mm'}(\boldsymbol{K},t)} + \mathrm{c.c.} \tag{3}$$

The intra-band current and the inter-band current are expressed as[14]

$$\boldsymbol{j}_{\mathrm{ra}}(t) = \sum_m \int_{\mathrm{BZ}} \boldsymbol{v}_m[\boldsymbol{K}+\boldsymbol{A}(t)]n_m(\boldsymbol{K},t)\,\mathrm{d}^3\boldsymbol{K}, \tag{4}$$

$$\boldsymbol{j}_{\mathrm{er}}(t) = \frac{\mathrm{d}}{\mathrm{d}t}\sum_{m\neq m'}\int_{\mathrm{BZ}}\boldsymbol{p}_{mm'}(\boldsymbol{K},t)\,\mathrm{d}^3\boldsymbol{K}, \tag{5}$$

where $\boldsymbol{v}_m(\boldsymbol{k}) = \nabla_{\boldsymbol{k}}\varepsilon_m(\boldsymbol{k})$ denotes the velocity of valence band $(m=\mathrm{v})$ and conduction band $(m=\mathrm{c})$. The intra-band and inter-band harmonic spectra are obtained by taking the Fourier transform of the intra-band current and inter-band current after derivation of time, respectively, and the total harmonic spectrum is obtained from the total currents:

$$I_{\mathrm{HHG}}(\omega) = |\omega^2\mathrm{FFT}[j_{\mathrm{ra}}(t) + j_{\mathrm{er}}(t)]|^2. \tag{6}$$

The one-dimensional SBE is adopted for simulation, and laser field can be expressed as

$$E(t) = E_0 f(t)\cos(\omega_0 t + \varphi_0 + \alpha t^2) + \beta E_0, \tag{7}$$

$$f(t) = \mathrm{e}^{-2(\ln 2)\frac{t^2}{\tau^2}}, \tag{8}$$

where $f(t)$ is a Gaussian type envelope, τ is the full width at half maximum (FWHM). E_0, ω_0, and φ_0 are the peak value, frequency, and carrier envelope phase of electric field, respectively; α is the chirped parameter; β is the amplitude ratio between the static electric field and the fundamental frequency field (E_0). The polarization direction of the laser pulse is along the Γ–M direction of ZnO crystal.

In solid, electrons (holes) move according to Newtonian equations: $\frac{\mathrm{d}}{\mathrm{d}t}(\hbar\boldsymbol{k}) = \boldsymbol{E}(t)$, where $\hbar\boldsymbol{k}$ is the momentum. The details are as follows:

The velocity of the electron (hole) is $\boldsymbol{v} = \frac{1}{\hbar}\nabla_{\boldsymbol{k}}\varepsilon(\boldsymbol{k})$, where $\varepsilon(\boldsymbol{k})$ is the energy of the band. The acceleration is $\boldsymbol{a}(t) = \boldsymbol{F}/m = -q\boldsymbol{E}(t)/m = -\boldsymbol{E}(t)$ (in atomic units, $\hbar = q = m = 1$) and $\boldsymbol{a}(t) = \mathrm{d}\boldsymbol{v}(t)/\mathrm{d}t$, thus $\mathrm{d}\boldsymbol{v}(t)/\mathrm{d}t = -\boldsymbol{E}(t)$. The momentum is $\boldsymbol{k}(t) = m\boldsymbol{v}$, so $\mathrm{d}\boldsymbol{k}(t)/\mathrm{d}t = -\boldsymbol{E}(t)$. By integrating both sides with respect to time $\int_{t'}^{t}\frac{\mathrm{d}\boldsymbol{k}(t'')}{\mathrm{d}t''}\,\mathrm{d}t'' = -\int_{t'}^{t}\boldsymbol{E}(t'')\,\mathrm{d}t''$, we get $\boldsymbol{k}(t) - \boldsymbol{k}(t') = \boldsymbol{A}(t) - \boldsymbol{A}(t')$. Furthermore, the reciprocal space trajectory of the ionized electron (hole) from time t' can be obtained as $\boldsymbol{k}(t) = \boldsymbol{k}_0 + \boldsymbol{A}(t) - \boldsymbol{A}(t')$.

The intraband current and interband current can be calculated by the solid strong field approximation formula[14]

$$\begin{aligned}\boldsymbol{J}_{\mathrm{ra}}(\omega) =& \sum_{m=\mathrm{c,v}} s_m\int_{-\infty}^{\infty}\mathrm{d}t\,\mathrm{e}^{-\mathrm{i}\omega t}\Big[\int_{\mathrm{BZ}}\mathrm{d}^3\boldsymbol{k}\boldsymbol{v}_m(\boldsymbol{k}) \\ &\times\int_{-\infty}^{t}\mathrm{d}t'\boldsymbol{E}(t')d^*(\boldsymbol{k}_{t'})\times\int_{-\infty}^{t'}\mathrm{d}t''\boldsymbol{E}(t'')d(\boldsymbol{k}_{t''}) \\ &\times\mathrm{e}^{\mathrm{i}S(\boldsymbol{k},t'',t')-(t'-t'')/T_2} + \mathrm{c.c.}\Big],\end{aligned} \tag{9}$$

$$\boldsymbol{J}_{\mathrm{er}}(\omega) = \omega\int_{-\infty}^{\infty}\mathrm{d}t\,\mathrm{e}^{-\mathrm{i}\omega t}\Big[\int_{\mathrm{BZ}}\mathrm{d}^3\boldsymbol{k}d^*(\boldsymbol{k})\int_{-\infty}^{t}\mathrm{d}t'\boldsymbol{E}(t')$$

$$\times d(\boldsymbol{k}_{t'})\,\mathrm{e}^{\mathrm{i}S(\boldsymbol{k},t',t)-(t-t')/T_2}+\mathrm{c.c.}\Big], \tag{10}$$

where $\boldsymbol{k}_{t'}=\boldsymbol{k}+\boldsymbol{A}(t')-\boldsymbol{A}(t)$, $S(\boldsymbol{k},t',t)=\int_{t'}^{t}\varepsilon_g(\boldsymbol{k}_\tau)\,\mathrm{d}\tau$.

In the solid strong field approximation theory, the contribution of interband polarization near the saddle point dominates. The phase term in the interband current is

$$\phi=S(\boldsymbol{k},t',t)-\omega t+\frac{\mathrm{i}(t-t')}{T_2}. \tag{11}$$

At the saddle point, the first derivative of the phase term with respect to the three variables $\boldsymbol{k},t',t$ is equal to 0, and the three saddle point equations can be given as follows:

$$\frac{\partial\phi}{\partial\boldsymbol{k}}=\nabla_{\boldsymbol{k}}S(\boldsymbol{k},t',t)=\Delta x(\boldsymbol{k},t',t)=x_{\mathrm{e}}-x_{\mathrm{h}}=0, \tag{12}$$

$$\frac{\partial\phi}{\partial t'}=\frac{\partial}{\partial t'}S(\boldsymbol{k},t',t)-\frac{\mathrm{i}}{T_2}=\varepsilon_g[\boldsymbol{k}+\boldsymbol{A}(t')-\boldsymbol{A}(t)]-\frac{\mathrm{i}}{T_2}=0, \tag{13}$$

$$\frac{\partial\phi}{\partial t}=\frac{\partial}{\partial t}S(\boldsymbol{k},t',t)-\omega+\frac{\mathrm{i}}{T_2}=\varepsilon_g(\boldsymbol{k})-\omega+\frac{\mathrm{i}}{T_2}=0. \tag{14}$$

Three saddle point equations are given, and three saddle point conditions can be obtained: (i) $\boldsymbol{k}(t)=\boldsymbol{k}_0+\boldsymbol{A}(t)-\boldsymbol{A}(t')$ denotes the electron tunneling from the minimum band gap $\boldsymbol{k}_0$ at time t', which is called the tunneling condition. (ii) $\Delta x_{\mathrm{e}}-\Delta x_{\mathrm{h}}=0$ represents the recollision of electrons and holes in real space, and the harmonic photons are emitted when the collision occurs, which is called the recollision condition. (iii) $\omega=\varepsilon_{\mathrm{c}}[\boldsymbol{k}(t)]-\varepsilon_{\mathrm{v}}[\boldsymbol{k}(t)]$ indicates that the energy of the harmonic photon radiated upon recollision is equal to the instantaneous band gap when the electron–hole pair recombines, which is called the energy conservation condition. If only (i) and (ii) are considered, the k-space quasi-classical model can be obtained. If (i), (ii), and (iii) are considered at the same time, the real space recollision model can be obtained. The real space recollision model holds that electrons undergo three processes, namely tunneling ionization, electron acceleration, and electron hole pair recombination, and finally we can realize harmonic radiation.[41]

3. Results and discussion

In our calculations, we use fundamental pulse ($\alpha=0$, $\beta=0$) with $E_0=0.0037$ a.u. ($I=0.48$ TW/cm^2), $\lambda=3200$ nm, $\omega_0=0.0142$ a.u., $\varphi_0=0$, and $\tau=10.3$ fs or $\tau=64$ fs. The chirp parameter α is selected to be 3×10^{-6} and 5×10^{-6}. The amplitude ratio between the static electric field and the fundamental frequency field, β, is chosen as 0.2 and 0.4. Although the static field of $\beta=0.4$ is slightly higher, it may be difficult to realize experimentally, but low-frequency laser field (such as CO_2 laser) can be used instead.[10,42,43] The total duration is taken as 4 o.c. and 25 o.c. (o.c.: optical cycle) in the simulation. Firstly, the structure top view of ZnO and the valence band and conduction band are shown in Figs. 1(a) and 1(b). Figure 1(a) shows the top view of ZnO in real space, which presents a hexagonal honeycomb structure. We focus on the band structure along the Γ–M direction of the crystal, as shown in Fig. 1(b), including a valence band and a conduction band, marked by solid line and dashed line, respectively. In order to compare the influence of chirp parameters and amplitude ratios of static electric field to fundamental frequency pulse on HHG, the harmonics under different parameters or amplitude ratios of fields are shown in Fig. 2.

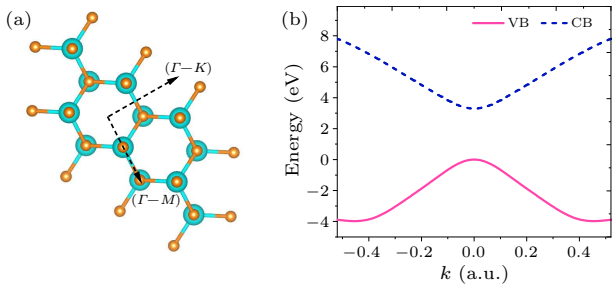


Fig. 1. (a) Top view of wurtzite ZnO with the Zn (the blue balls) and O (the orange balls) atoms. (b) Energy band structure of ZnO along the Γ–M direction, considering the two-band model with a valence band and a conduction band.

It can be seen from Figs. 2(a1) and 2(b1) that the harmonics drop rapidly from 0 to the 7th order, and the intensity of the harmonics is almost constant from 9th to 29th order, about 10^{-7} orders of magnitude, and the cutoff is of the 29th order. With the introduction of chirped pulse with 4 o.c. and 25 o.c. in Figs. 2(a1) and 2(b1), we can see that harmonic modulation is obvious. Moreover, the existence of static electric field can improve the harmonic efficiency, as shown in Figs. 2(a2) and 2(b2). When the combination of single-color chirp-free pulse and static electric field is considered ($\alpha=0$, $\beta\neq0$), the modulation in the harmonic platform is reduced, and the interference structure of harmonics below the 7th order is obvious. Driven by the combination of single-color chirped pulse and static electric field, we can obtain relatively continuous harmonic spectrum. Compared with the 4-period case, the harmonic spectrum presents similar characteristic with the 25-period case. Furthermore, we also consider the influence of the combined pulse of chirped pulse and static electric field on HHG, and find that the harmonic intensity in Figs. 2(a3) and 2(b3) is roughly 1 or 2 orders of magnitude higher than that in Figs. 2(a1) and 2(b1). However, compared to HHG driven by the combination of single-color chirp-free pulse and static electric field in Figs. 2(a2) and 2(b2), the modulation of the harmonic driven by the combination of chirped pulse and static electric field is more obvious [as shown in Figs. 2(a3) and 2(b3)].

The harmonics are optimized. By changing the laser intensity of the single-color chirp-free field, the peak intensity of the electric field reaches the peak intensity of the combination of the single-color field and the static electric field

($E_0 = 0.0044$ a.u., $E_{01} = 0.0051$ a.u.), and calculating the harmonic spectrum in Figs. 3(a) and 3(b), we find that the harmonic intensity is improved. When the static electric field is added, the harmonic efficiency is indeed improved and relatively continuous harmonic spectra are obtained with the 4-period and 25-period cases, and with the 4-period case the harmonics are smoother. Moreover, by changing the carrier envelope phase (CEP) of the single-color chirp-free laser pulse, harmonics are seldom changed, which is not shown.

The harmonic spectrum is calculated when the amplitude ratio of the static electric field to the fundamental laser field is negative ($\beta = -0.2$, $\beta = -0.4$), as shown in Fig. 4. We can find that the harmonic efficiency is improved no matter whether β is positive or negative. However, when positive values are taken, relatively continuous harmonics can be obtained.

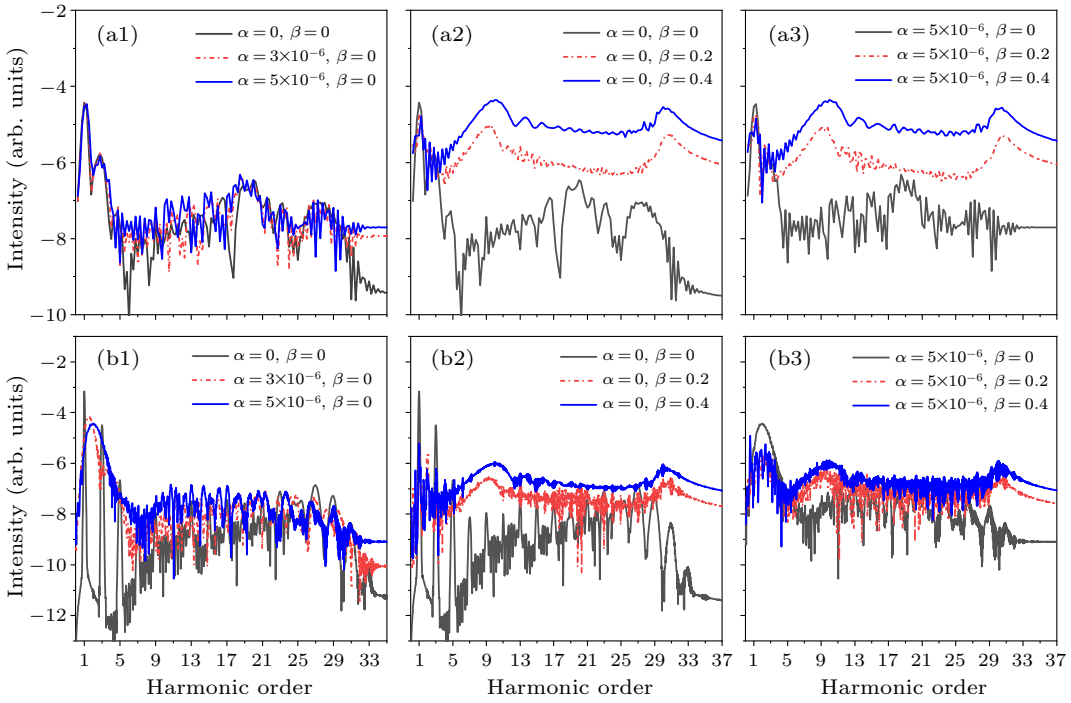


Fig. 2. HHG from ZnO driven by different fields in 4-period and 25-period cases. (a1)–(a3) HHG in the single-color chirped pulse ($\alpha = 3 \times 10^{-6}, 5 \times 10^{-6}$), the combination of single-color chirp-free pulse and static electric field ($\beta = 0, 0.2, 0.4$), and the combination of single-color chirped pulse and static electric field with duration of 4 optical cycles. (b1)–(b3) Results with pulse duration of 25 optical cycles. Other laser parameters are the same as those in (a1)–(a3).

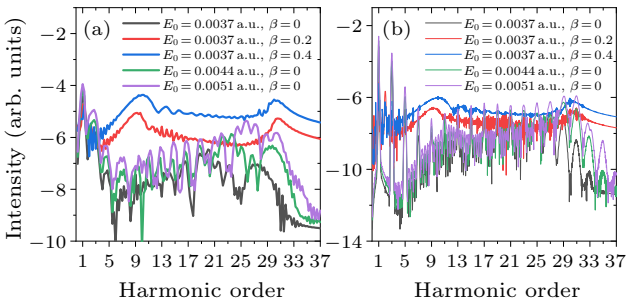


Fig. 3. The total harmonic spectrum under the laser field with (a) 4 o.c. and (b) 25 o.c. at different laser intensities.

In the case of HHG in gas, the introduction of chirp pulse and static electric field can greatly improve the cutoff frequency,[11,44,45] and enhance the harmonic efficiency.[46,47] However, in our work, the intensity of the harmonic plateau is improved, but the cutoff cannot be extended. This phenomenon is quite different from the results of HHG in gas. In order to analyze the internal reasons for these differences, we first give the profile and vector potential of each field, and the time-dependent electron population in the conduction band. For the convenience of the analysis, we only consider the 4-period case.

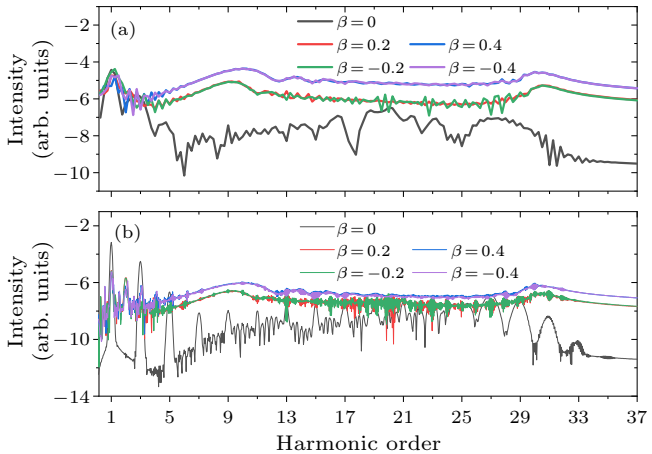


Fig. 4. The harmonic spectrum under the combination of the single-color pulse and static electric field with different amplitude ratios ($\beta = 0$, $\beta = 0.2$, $\beta = 0.4$, $\beta = -0.2$, $\beta = -0.4$): (a) 4 o.c., (b) 25 o.c.

Figure 5 shows the electric field profiles of different laser fields, the vector potential, and the electron population of con-

duction band. We can see that with static electric field, the ionization probability of electron is greater than that of single-color chirp free pulse and chirped pulse. The fast excitation of electrons is still related to the peak value of electric field and corresponding vector potential. When the electric field reaches its peak value and the value of the corresponding vector potential is not 0, the electron is rapidly excited to the conduction band [see Fig. 5(b)]. Because the addition of the static electric field breaks the symmetry of the field in the adjacent half period, the maximum peak value of the laser field increases, so that the probability of electron ionization increases [see Figs. 5(a) and 5(c)].

In order to clearly understand the physical mechanism of the large difference between the harmonic spectra in ZnO and the gas, we present the time-frequency of the harmonics in ZnO. Based on the change of the field waveform and the rapid excitation rate of electrons at the peak value of the electric field, the harmonic spectrum in Fig. 2 is further analyzed in combination with the time frequency, as shown in Fig. 6. The harmonics mainly contribute from short trajectories by a single-color chirp free pulse in Fig. 6(a). By introducing the chirped pulse, the contribution of long quantum trajectories is enhanced, leading to the appearance of modulation in the harmonics, and the interference structure is evident in Fig. 6(b), which is consistent with the harmonic spectrum in Fig. 2(a1). Similar results can be obtained in the case of 25 o.c.

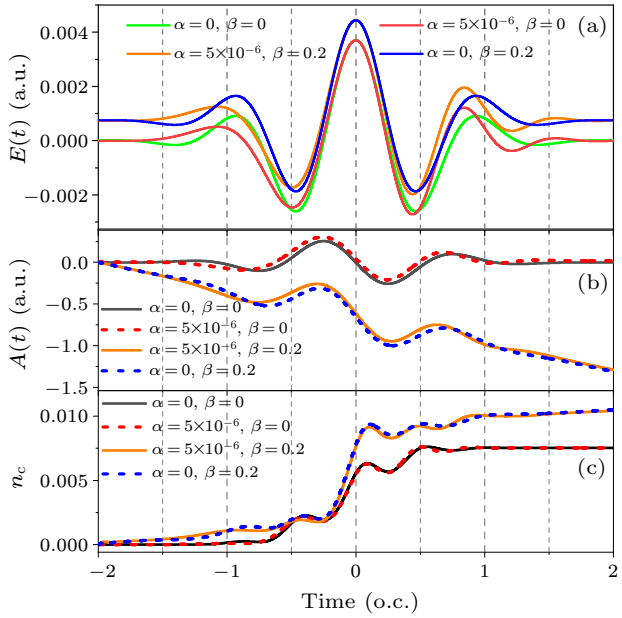


Fig. 5. (a) Electric field profiles of single-color chirp free pulse, single-color chirped pulse, combination of single-color chirp free pulse and static electric field, and combination of single-color chirped pulse and static electric field. (b) The vector potential corresponding to (a). (c) Evolution of electron population in conduction band as a function of time in each field.

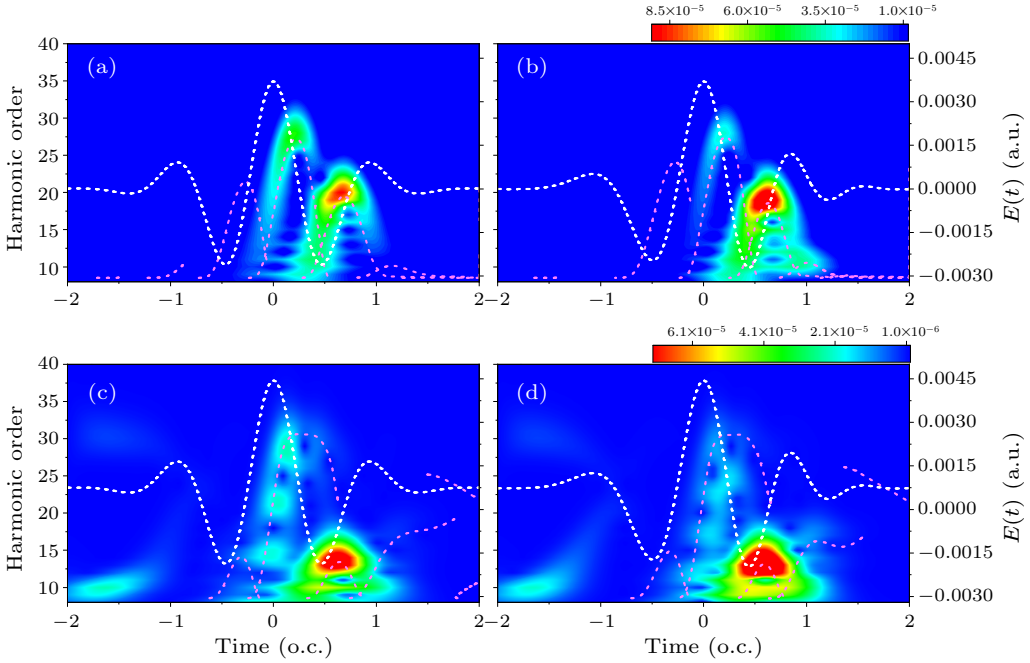


Fig. 6. The time-frequency distribution of HHG driven by (a) single-color chirp free linearly polarized laser field, (b) single-color chirped pulse ($\alpha = 5 \times 10^{-6}$), (c) the combination of single-color chirp-free pulse and static electric field ($\beta = 0.2$), and (d) the combination of single-color chirped pulse and static electric field ($\alpha = 5 \times 10^{-6}$, $\beta = 0.2$). The electric field profile (white dashed line) and the classical trajectory (pink dashed line) are given.

In the case of 4 o.c., the main contribution of harmonics is from short trajectories when ZnO is driven by single-color chirp-free pulse and there are mainly two peaks in the time-frequency distribution of harmonics. Some electrons are excited to the conduction band at $t = -0.5$ o.c. and return to the valence band around $t = 0$ o.c., radiating harmonics, corresponding to harmonic peaks of the time-frequency distribution around $t = 0$ o.c. The harmonic peak around $t = 0.5$ o.c. mainly stems from the fast excitation of electrons at $t = 0$ o.c. when the pulse reaches its peak. The time frequency agrees

well with the classical recollision trajectory in Fig. 6. In Fig. 6(b), compared with the chirp free pulse, the amplitude and frequency of the chirp pulse are smaller, and the probability of electron ionization is lower at $t < 0$ o.c. As a result, the probability of electron returning to valence band and recombination with hole after $t = 0$ o.c. is reduced, and the harmonic signal of radiation is weakened. Corresponding to Figs. 2(a1) and 2(b1), the intensity of the high-energy region of harmonics decreases slightly. However, the strong signal of harmonic peak around $t = 0.5$ o.c. is mainly due to tunneling excitation of electrons at $t = 0$ o.c., when the laser field reaches its peak, and the probability of electron ionization reaches its maximum. At $t = 0.5$ o.c., the amplitude and instantaneous frequency of the chirp field increase, then the possibility of recollision of electron–hole pairs increases, and the emitted harmonic signal is enhanced, which leads to a slightly increase in the intensity of the harmonic plateau as shown in Figs. 2(a1) and 2(b1).

In Figs. 6(c) and 6(d), in the presence of static electric field, for low order harmonics, both long and short quantum trajectories have important contribution, corresponding to strong harmonic spectrum modulation.[40] For the part larger than 17th order, the short trajectory makes the great contribution to HHG, and the long trajectory is largely suppressed, corresponding to relatively continuous harmonic spectrum in Figs. 2(a2) and 2(a3) and Figs. 2(b2) and 2(b3).

The total harmonic spectrum is mainly contributed by the inter-band harmonic spectrum, so we also give k-resolved profile of the inter-band harmonic spectra analyzed by a four-step model.

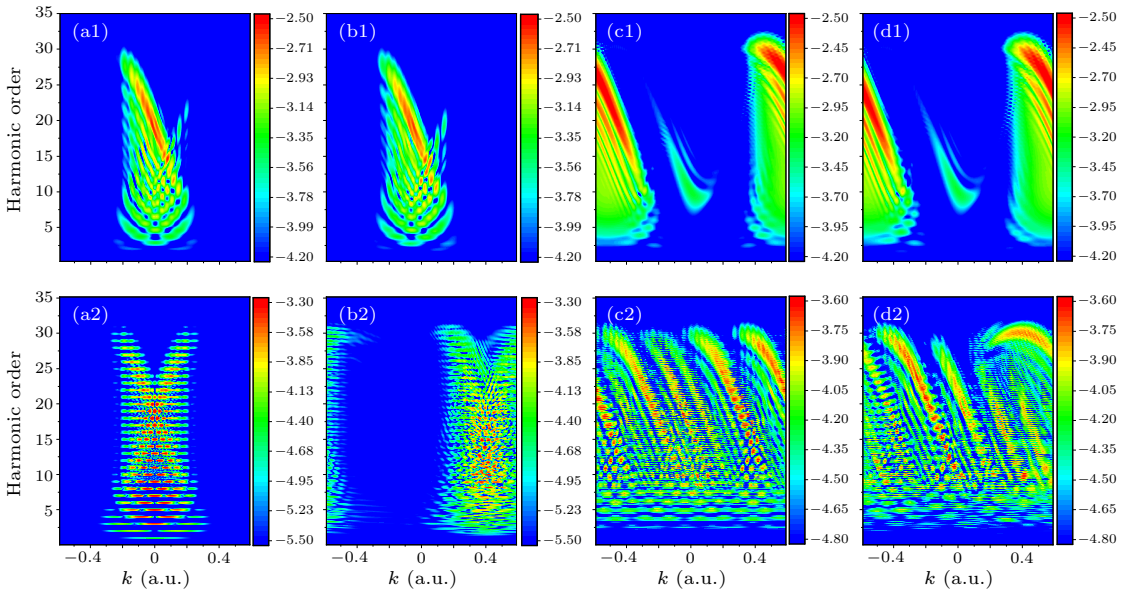


Fig. 7. The k-resolved profile of inter-band harmonic spectra generation by different fields. (a1)–(d1) The k-resolved profile of inter-band harmonic spectra by single-color chirp-free pulse ($\alpha = 0$, $\beta = 0$), single-color chirped pulse ($\alpha = 5 \times 10^{-6}$), the combination of single-color chirp-free pulse and static electric field ($\beta = 0.2$), and the combination field of single-color chirped pulse and static electric field ($\alpha = 5 \times 10^{-6}$, $\beta = 0.2$) with the duration of 4 o.c. (a2)–(d2) Results with a pulse duration of 25 o.c. Other parameters are the same as those in (a1)–(d1).

Figures 7(a1)–7(d1) and 7(a2)–7(d2) show the k-resolved inter-band harmonic spectra for a single-color chirp free pulse, a single-color chirped pulse, a combined field of single-color chirp free pulse and static electric field, and a combined field of single-color chirped pulse and static electric field with 4 o.c. and 25 o.c., respectively. In the case of 4 o.c., some electrons whose initial momentum is not 0 move to the top of the valence band driven by the laser field, and this is called the pre-acceleration process. The electrons that reach the top of the valence band will be excited to the bottom of the conduction band more easily, and the electrons excited to the conduction band and the holes in the valence band will undergo Bloch oscillation together in the laser field. Since the peak values of laser pulses in the adjacent half periods are different, the electrons moving on the conduction band will move at different distances on both sides of the Γ point. In adjacent half-cycle, when the peak value of pulse is small, electron–hole pairs are driven to move near $k = 0$, while the peak value of pulse is large, electron–hole pairs are driven to move far away from $k = 0$, resulting in incomplete X-type structures of k-resolved inter-band harmonic spectra in Figs. 7(a1)–7(d1). In the case of 25-period single-color chirp free pulse as shown in Fig. 7(a2) and single-color chirped pulse as shown in Fig. 7(b2), the k-resolved inter-band harmonics presents the X-type structure. Under the chirped pulse, the inter-band harmonic spectrum in k-space is asymmetric with respect to $k = 0$. After the static electric field is added, k-resolved inter-band harmonic spectrum has a periodic incomplete X-type intensity distribution structure along the k direction [see Figs. 7(c2) and 7(d2)]. Due to the introduction of 25-period pulses, k-resolved

inter-band harmonic spectrum shows a periodic sloping structure as shown in Figs. 7(c1) and 7(c2) and Figs. 7(d1) and 7(d2).

Incomplete X-type k-resolved profile of interband harmonic spectrum can be explained by the four-step model. In Figs. 8(a1)–8(a3), we can see that the electron tunnels from the top of the valence band at $t = 0$ o.c., and then presents Bloch oscillation in the conduction band. At $t = 0.25$ o.c., vector potential reaches its peaks at -0.2573 a.u., and the electron moves to $k(t) = -0.2573$ a.u. At $t = 0.55$ o.c., the vector potential is approximately 0 and the electron returns to the bottom of the conduction band. At $t = 0.75$ o.c., the vector potential reaches peak of 0.0988 a.u., and the electron also moves to the $k(t) = 0.0988$ a.u. In addition, the electrons have a pre-acceleration process in the valence band before tunneling. Therefore, in the case of 4 o.c., the k-resolved inter-band harmonics finally present an incomplete X-shaped structure as shown in Fig. 7(a1). In the 4-period single-color chirped field (see Figs. 8(b1)–8(b3)), the asymmetric X-type structure can also be analyzed by the motion of electrons in k-space. Before $t = 0.026$ o.c., the electron near the top of the valence band goes through a pre-acceleration process to $k = 0$ a.u. and then the electrons are excited at $t = 0.026$ o.c. At $t = 0.24$ o.c., the vector potential reaches a peak of -0.2088 a.u. and the electron moves to $k(t) = -0.2088$ a.u. The electron then accelerates. The vector potential is 0 and the electron returns to the bottom of the conduction band at $t = 0.48$ o.c. At $t = 0.68$ o.c., the vector potential reaches another peak of 0.1197 a.u., and the electron also moves to the $k(t) = 0.1197$ a.u. The velocity of the electron decreases to 0 and returns to the lowest point of the conduction band, and then reaches the bottom of the conduction band at $t = 1$ o.c.

In the presence of static electric field, the asymmetric motion of electrons with the change of laser field and vector potential can also be analyzed. Because the static electric field greatly breaks the symmetry of the laser field, k-resolved interband harmonic spectrum only reflects a part of the X-type structure.

In order to visualize how the laser field affects the electron trajectory, we present the population of transient conduction band. In the 4-period case [see Figs. 9(a1)–9(d1)], the electron Bloch oscillation is small, while in the 25-period case, the oscillation is significant [see Figs. 9(a2)–9(d2)], and the electron Bloch oscillation is much stronger when the chirped pulse is introduced in Figs. 9(b1) and 9(b2) and Figs. 9(d1) and 9(d2). Introducing the static electric field, the region reflecting the electrons oscillating is wider, and electrons cross the edge of the first Brillouin zone and experience a Bragg reflection, superimposing the Bloch oscillations[15,24,35,48,49] in the band [see Figs. 9(c1) and 9(c2) and Figs. 9(d1) and 9(d2)], so that the radiation of multi-channel harmonics occurs, which plays an important role in promoting the harmonic efficiency. The k-resolved inter-band harmonics in Figs. 7(c1) and 7(c2) and Figs. 7(d1) and 7(d2) show a periodic slope structure.

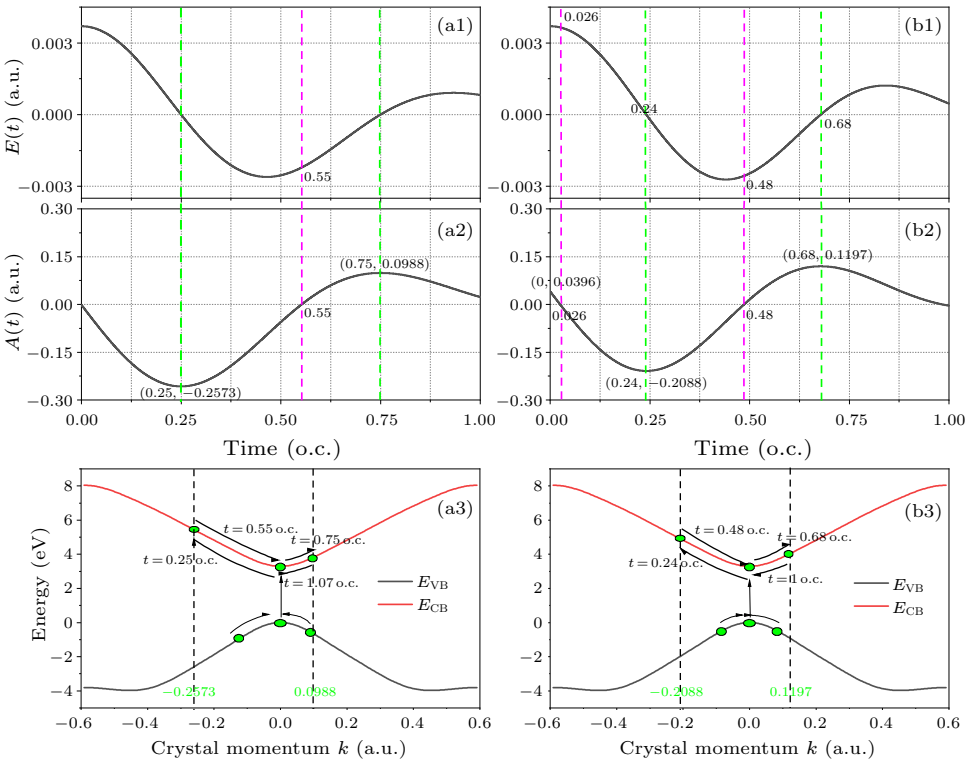


Fig. 8. The electric field and vector potential of [(a1), (a2)] single-color chirp-free pulse and [(b1), (b2)] single-color chirped pulse in single cycle. Schematic diagram of the motion of the electron driven by (a3) a single-color chirp-free pulse and (b3) a single-color chirped pulse in k-space.

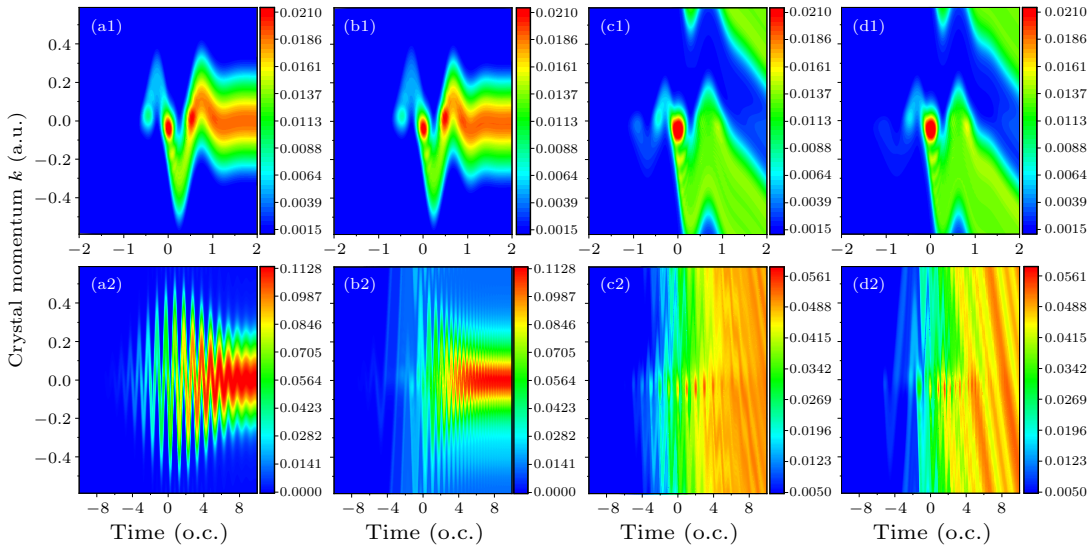


Fig. 9. The time-dependent population of conduction band by laser pulse with (a1)–(d1) 4 o.c. and (a2)–(d2) 25 o.c.

In Figs. 9(a1)–9(d1), in the 4-period case, it can be seen that the asymmetry of the electron oscillation in k-space is consistent with the asymmetry of the electron motion analyzed in Fig. 8. Electrons travel longer distances along the negative half axis and shorter distances along the positive half axis of the crystal momentum in k-space. This also corresponds to the X-type structure with asymmetric k-resolved inter-band harmonic spectra in Figs. 7(a1)–7(d1). However, in the case of 25-period [see Figs. 9(a2) and 9(b2)], due to the presence of the pre-acceleration process and the conservation of energy, the corresponding k-resolved inter-band harmonic spectrum shows a relatively symmetric X-type structure [see Figs. 7(a2) and 7(b2)].

4. Conclusions

We have studied HHG in ZnO crystals under chirped field and static electric field with 4 o.c. and 25 o.c. In the single-color chirped laser field, the harmonic cutoff does not extend, but the interference structure is enhanced. In the presence of the static electric field, the harmonic cutoff also remains unchanged, but the harmonic efficiency is improved. The obvious interference structure of harmonics originates from the interference between short and long trajectories, while the continuous harmonics larger than the 17th order in the static electric field are mainly contributed by the short trajectories. By analyzing the motion of electrons in k space, we explain the incomplete X-type structure of the harmonic spectrum in the asymmetric chirped pulse and static electric field. By single-color chirp-free pulses with 25 cycles, k-resolved inter-band harmonic spectrum exhibits a complete X-shaped structure, which reflects the energy conservation and pre-acceleration process. Because the two peak values of the laser field in adjacent half periods have different sizes, resulting in different movement distances of electrons on both sides of the Γ point, the k-resolved inter-band harmonic spectrum presents an incomplete X-type intensity distribution structure. At the same time, we also explain the existence of the pre-acceleration process. In the presence of the static electric field, electrons cross the first BZ and experience a Bragg reflection, as well as a superposition of oscillation in the conduction band, thus resulting in the radiation of multi-channel harmonics. In addition, time-dependent conduction band population is given, which is consistent with the electron motion in the conduction band.

Acknowledgments

This work was supported by the Natural Science Foundation of Jilin Province (Grant No. 20220101010JC) and the National Natural Science Foundation of China (Grant No. 12074146).

References

[1] Bian X B and Bandrauk A D 2010 *Phys. Rev. Lett.* **105** 093903
[2] Krausz F and Ivanov M 2009 *Rev. Mod. Phys.* **81** 163
[3] Corkum P B 1993 *Phys. Rev. Lett.* **71** 1994
[4] Li L, Lan P F, Zhu X S, Huang T F, Zhang Q B, Lein M and Lu P X 2019 *Nat. Phys.* **122** 193901
[5] Song X H, Yang S D, Zuo R X, Meier T and Yang W F 2020 *Phys. Rev. A* **101** 033410
[6] Ciappina M F, Pérez-Hernández J A, Landsman A S, Okell W A, Zherebtsov S, Förg B, Schötz J, Seiffert L, Fennel T, Shaaran T, Zimmermann T, Chacón A, Guichard R, Zaïr A, Tisch J W G, Marangos J P, Witting T, Braun A, Maier S A, Roso L, Krüger M, Hommelhoff P, Kling M F, Krausz F and Lewenstein M 2017 *Rep. Prog. Phys.* **80** 054401
[7] Chen J G, Zeng S L and Yang Y J 2010 *Phys. Rev. A* **82** 043401
[8] Feng L and T Chu 2011 *Phys. Rev. A* **84** 053853
[9] Koushki A M and Sarikhani S 2021 *Chem. Phys.* **541** 111020
[10] Xiang Y, Niu Y P and Gong S Q 2009 *Phys. Rev. A* **79** 053419
[11] Mohebbi M 2016 *Appl. Phys. B* **122** 39
[12] Liu H, Feng L Q, Qiao Y and Li Y 2021 *J. Mod. Opt.* **68** 267
[13] Vampa G and Brabec T 2017 *J. Phys. B: At. Mol. Opt. Phys.* **50** 083001
[14] Vampa G, McDonald C R, Orlando G, Klug D D, Corkum P B and Brabec T 2014 *Phys. Rev. Lett.* **113** 073901

[15] Du T Y, Tang D, Huang X H and Bian X B 2018 *Phys. Rev. A* **97** 043413
[16] Ghimire S and Reis D A 2018 *Nat. Phys.* **15** 10
[17] Yue L and Gaarde M B 2020 *Phys. Rev. Lett.* **124** 153204
[18] He Y L, Guo J, Gao F Y, Yang Z J, Zhang S Q and Liu X S 2021 *Phys. Rev. A* **104** 013104
[19] Wang X Q, Xu Y, Huang X H and Bian X B 2018 *Phys. Rev. A* **98** 023427
[20] Hawkins P G, Ivanov M Y and Yakovlev V S 2015 *Phys. Rev. A* **91** 013405
[21] Jin J Z, Xiao X R, Liang H j, Wang M, Chen S G, Gong Q H and Peng L Y 2018 *Phys. Rev. A* **97** 043420
[22] Li J B, Zhang X, Yue S J, Wu H M, Hu B T and Du H C 2017 *Opt. Express* **25** 18603
[23] Liu X, Zhu X S, Lan P F, Zhang X F, Wang D, Zhang Q B and Lu P X 2017 *Phys. Rev. A* **95** 063419
[24] Mücke O D 2011 *Phys. Rev. B* **84** 081202
[25] Wu M X, Ghimire S, Reis D A, Schafer K J and Gaarde M B 2015 *Phys. Rev. A* **91** 043839
[26] Floss I, Lemell C, Wachter G, Smejkal V, Sato S A, Tong X M, Yabana K and Burgdörfer J 2018 *Phys. Rev. A* **97** 011401
[27] Le Breton G, Rubio A and Tancogne-Dejean N 2018 *Phys. Rev. B* **98** 165308
[28] Otobe T 2016 *Phys. Rev. B* **94** 235152
[29] Tancogne-Dejean N, Mücke O D, Kärtner F X and Rubio A 2017 *Nat. Commun.* **8** 745
[30] Tancogne-Dejean N, Mücke O D, Kärtner F X and Rubio A 2017 *Phys. Rev. Lett.* **118** 087403
[31] Alam D, Ud Din N, Chini M and Turkowski V 2022 *Phys. Rev. B* **106** 235124
[32] Golde D, Meier T and Koch S W 2008 *Phys. Rev. B* **77** 075330
[33] Jiang S C, Chen J G, Wei H, Yu C, Lu R F and Lin C D 2018 *Phys. Rev. Lett.* **120** 253201
[34] Jiang S C, Wei H, Chen J G, Yu C, Lu R F and Lin C D 2017 *Phys. Rev. A* **96** 053850
[35] McDonald C R, Vampa G, Corkum P B and Brabec T 2015 *Phys. Rev. A* **92** 033845
[36] Vampa G, Hammond T J, Thiré N, Schmidt B E, Légaré F, McDonald C R, Brabec T, Klug D D and Corkum P B 2015 *Phys. Rev. Lett.* **115** 193603
[37] Wang G and Du T Y 2021 *Phys. Rev. A* **103** 063109
[38] Qiao Y, Chen J Q, Huo Y Q, Liang H Q, Yu R X, Chen J G, Liu W J, Jiang S C and Yang Y J 2023 *Phys. Rev. A* **107** 023523
[39] Du T Y, Tang D and Bian X B 2018 *Phys. Rev. A* **98** 063416
[40] Shao T J, Lü L J, Liu J Q and Bian X B 2020 *Phys. Rev. A* **101** 053421
[41] Lang Y, Peng Z Y and Zhao Z X 2022 *Chin. Phys. Lett.* **39** 114201
[42] Borca B, Flegel A V, Frolov M V, Manakov N L, Milošević D B and Starace A F 2000 *Phys. Rev. Lett.* **85** 732
[43] Hong W Y, Lu P X, Cao W, Lan P F and Wang X L 2007 *J. Phys. B: At. Mol. Opt. Phys.* **40** 2321
[44] Zhang H D, Liu X W, Jin F C, Zhu M, Yang S D, Dong W H, Song X H and Yang W F 2021 *Chin. Phys. Lett.* **38** 063201
[45] Xu J J, Zeng B and Yu Y L 2017 *Phys. Rev. A* **82** 053822
[46] Peng D, Frolov M V, Pi L W and Starace A F 2018 *Phys. Rev. A* **97** 053414
[47] Feng L Q and Liu H 2022 *Chem. Phys. Lett.* **791** 139398
[48] You Y S, Wu M X, Yin Y C, Chew A, Ren X M, Gholam-Mirzaei S, Browne D A, Chini M, Chang Z H, Schafer K J, Gaarde M B and Ghimire S 2017 *Opt. Lett.* **42** 1816
[49] Zhang X, Li J B, Zhou Z S, Yue S J, Du H C, Fu L B and Luo H G 2019 *Phys. Rev. B* **99** 014304